Accepted Manuscript

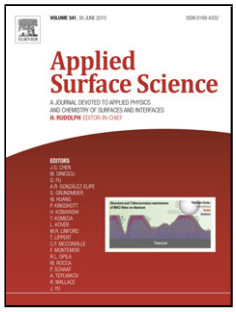

Title: Synthesis of core-shell hematite (α-Fe_2O_3) nanoplates: quantitative analysis of the particle structure and shape, high coercivity and low cytotoxicity

Authors: Marin Tadic, Lazar Kopanja, Matjaz Panjan, Slavko Kralj, Jasmina Nikodinovic-Runic, Zoran Stojanovic

PII: S0169-4332(17)30116-2
DOI: http://dx.doi.org/doi:10.1016/j.apsusc.2017.01.115
Reference: APSUSC 34910

To appear in: *APSUSC*

Received date: 20-7-2016
Revised date: 10-1-2017
Accepted date: 12-1-2017

Please cite this article as: Marin Tadic, Lazar Kopanja, Matjaz Panjan, Slavko Kralj, Jasmina Nikodinovic-Runic, Zoran Stojanovic, Synthesis of core-shell hematite (α-Fe2O3) nanoplates: quantitative analysis of the particle structure and shape, high coercivity and low cytotoxicity, Applied Surface Science http://dx.doi.org/10.1016/j.apsusc.2017.01.115

Synthesis of core-shell hematite (α-Fe_2O_3) nanoplates: quantitative analysis of the particle structure and shape, high coercivity and low cytotoxicity

Marin Tadic[1,*], Lazar Kopanja[2,3], Matjaz Panjan[4], Slavko Kralj[4], Jasmina Nikodinovic-Runic[5], Zoran Stojanovic[6]

[1]Condensed Matter Physics Laboratory, Vinca Institute, University of Belgrade, POB 522, 11001 Belgrade, Serbia

[2]Faculty of Mathematics and Computer Science, Alfa BK University, Palmira Toljatija 3, 11070 Belgrade, Serbia

[3]Faculty of Technology and Metallurgy, University of Belgrade, Karnegijeva 4, PO Box 3503, 11120 Belgrade, Serbia

[4]Jožef Stefan Institute, Jamova 39, 1000 Ljubljana, Slovenia

[5]Institute of Molecular Genetics and Genetic Engineering, University of Belgrade, Vojvode Stepe 444a, 11000 Belgrade, Serbia

[6]Institute of Technical Sciences, Serbian Academy of Arts and Sciences, Knez Mihajlova 35/IV, 11000 Belgrade, Serbia

[*]**Corresponding author:** Marin Tadic

Mailing address: Condensed Matter Physics Laboratory, Vinca Institute, University of Belgrade, P.O. Box 522, 11001 Belgrade, Serbia.

Phone: +381-11-6308828, Fax: +381-11-6308829

e-mail: marint@vinca.rs

Graphical abstract

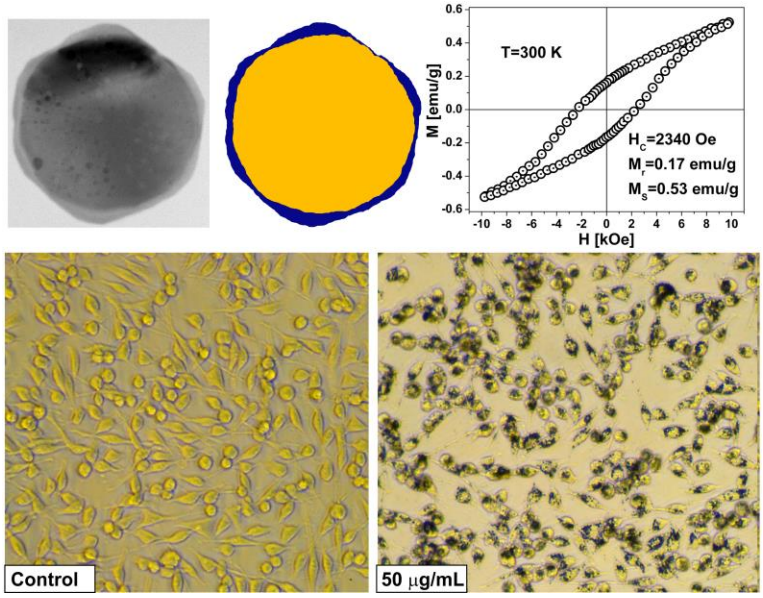

Highlights

- Uniform plate-like nanopartices are synthesized by hydrothermal method.
- Low-citotoxicity of hematite nanoplates is observed.
- High coercivity of the sample point to the shape anisotropy.
- Shape and structure of the nanoplates are analysed by computational methods.

Abstract

Hematite core-shell nanoparticles with plate-like morphology were synthesized using a one-step hydrothermal synthesis. An XRPD analysis indicates that the sample consist of single-phase α-Fe_2O_3 nanoparticles. SEM and TEM measurements show that the hematite sample is composed

of uniform core-shell nanoplates with 10–20 nm thickness, 80–100 nm landscape dimensions (aspect ratio ~5) and 3-4 nm thickness of the surface shells. We used computational methods for the quantitative analysis of the core–shell particle structure and circularity shape descriptor for the quantitative shape analysis of the nanoparticles from TEM micrographs. The calculated results indicated that a percentage of the shell area in the nanoparticle area (share [%]) is significant. The determined values of circularity in the perpendicular and oblique perspective clearly show shape anisotropy of the nanoplates. The magnetic properties revealed the ferromagnetic-like properties at room temperature with high coercivity H_C=2340 Oe, pointing to the shape and surface effects. These results signify core-shell hematite nanoparticles' for practical applications in magnetic devices. The synthesized hematite plate-like nanoparticles exhibit low cytotoxicity levels on the human lung fibroblasts (MRC5) cell line demonstrating the safe use of these nanoparticles for biomedical applications.

Keywords: hematite (α-Fe_2O_3), iron oxide, magnetic materials, surface effects, image analysis, cytotoxicity.

1. Introduction

Nanosized iron oxide polymorphs (α-Fe_2O_3, γ-Fe_2O_3, Fe_3O_4, β-Fe_2O_3 and ε-Fe_2O_3) have been the subject of numerous studies in the past ten years due to their unique structural properties, complex magnetic properties and the great diversity of practical applications [1-10]. Key requirements for the safe use of these nanomaterials for practical applications are low toxicity and high stability. The synthesis conditions must be well controlled to obtain fine powders of chosen polymorph with a narrow particle size distribution. Moreover, uniform shapes of the

nanoparticles are required in order to achieve specific physical properties convenient for specific applications.

Among iron oxide polymorphs, hematite is the most stable polymorph in the air, highly resistant to corrosion, has low toxicity and cost, and is environmentally friendly. Recent papers describe hematite's wide range of potential applications, such as catalysis, gas sensors, pigments, solar cells, lithium-ion batteries, magnetic and antibacterial materials [11-18]. To modify or improve its physical properties, the focus is on the preparation of the nanosized α-Fe_2O_3. Until now, various synthesis methods have been developed to prepare hematite materials, involving solid-state reactions, sol–gel process, hydrothermal synthesis, solvothermal method, polyol process, mechanical activation, coprecipitation and template method [11,19-28]. The study of the magnetic properties of nanosized hematite particles is of great importance from fundamental and applications points of view. Nanosized hematite is an interesting material for investigation of magnetic properties because it can display antiferromagnetic, weak-ferromagnetic and superparamagnetic properties. The bulk α-Fe_2O_3 compound is antiferromagnetic below a Morin temperature (T_M=263 K), whereas above the T_M, the hematite is weak-ferromagnet with a Neel temperature about 956 K [11]. The Neel and Morin temperatures of the α-Fe_2O_3 nanoparticle are size dependent and both decrease with decreasing particle size. Above the Neel temperature, hematite shows paramagnetic properties. If particles become small enough, the direction of the magnetic moment in a single domain fluctuates due to thermal agitation, leading to superparamagnetic behavior above the blocking temperature T_B, and to the spatial freezing of these moments below T_B [29,30].

Complex magnetic properties of hematite have been recently discussed and a wide range of magnetic properties has been obtained. The influence of the shape of the particles on the

coercivity is well known and the increase of the coercivity with increasing aspect ratio has been reported [11,31]. Therefore, the wide range of applications needs specific properties which can be tailored by the distinct size and the shape of α-Fe_2O_3 nanoparticles. Considering the applications of hematite material, various kinds of nanostructures have been prepared, such as nanocrystals, nanowires, nanobelts, nanotubes, nanorods, nanocubes, hollow nanospheres, plate-like particles etc. Jayashainy *et al.* reported that the coercivity of the α-Fe_2O_3 nanostructures can be influenced by the aspect ratio (AS) of the particles [31]. They suggested that the coercivity value has following trend: nanorods (H_C=483.29 Oe, AS~4.46) > nanotubes (H_C=321.96 Oe, AS~3) > nanotires (H_C=277.07 Oe, AS~1.39). Hence, the coercivity was found to increase with the aspect ratio. Roy *et al.* reported that the α-Fe_2O_3-Na microcubes rendered enhanced H_C (5.7 kOe) and M_R (0.203 emu g^{-1}) values at room temperature due to the shape and magnetocrystalline anisotropy, as well as increased strain in crystals in the presence of Na^+ ions within the crystal layers [32]. Li *et al.* also reported that the high aspect ratio enhances the shape anisotropy which in turn induces large magnetic coercivity [33]. Clearly, the shape of nanoparticles is important for improving the physical properties of the hematite. However, an important issue that still needs to be addressed in order to better understand shape-dependent properties is a unique method which can objectively measure the shape of the nanoparticles from the micrographs [34-38].

In this work, we report on the synthesis, magnetic properties, quantitative analysis of the particle structure and particle shape from TEM images as well as cytotoxicity of synthesized core-shell hematite nanoplates.

2. Experimental

All reagents were commercially acquired and used without further purification. The hematite nanoplates samples were synthesized by hydrothermal method. In 75 ml autoclave, we mixed 28.5 ml of ethanol (Sigma Aldrich) and 1.78 g of acetic acid (Sigma Aldrich). Afterwards, we added 0.83 g of $FeCl_3*6H_2O$ (Sigma Aldrich). Separately, 1.1872 g of NaOH (Sigma Aldrich) was dissolved in 2.1 ml of distilled water and 2 ml of 96 % ethanol. This solution was then added drop by drop under magnetic stirring in the autoclave to neutralize the acetic acid. The autoclave was sealed in digestion bomb and immersed in 180 $^{\circ}$C preheated oil bath. After 22 h of treatment, digestion bomb was pulled out of oil and left to cool down for a couple of hours in the air. Liquid phase was then carefully decanted from the autoclave and precipitates were collected. Collected nanoparticles were washed three times with distilled water, one time with ethanol and finally dried in hot air for ten hours.

The crystallinity and crystal phase of the synthesized nanoparticles were examined by X-ray powder diffraction (XRPD, Phillips PW-1710). The size and morphology of the synthesized sample were observed by scanning electron microscopy (SEM, JEOL JSM-7600F) and transmission electron microscopy (TEM, JEOL JEM-2100). Magnetic properties were measured by VSM magnetometer (Lake Shore 7307 VSM).

The cytotoxicity of the synthesized nanoparticles was assessed on human lung fibroblasts (MRC5) cell line obtained from the ATCC culture collection. The viability of cells was evaluated with 3-(4,5-dimethylthiazol-2-yl)-2,5-diphenyltetrazolium bromide reduction assay after 48 h of cell incubation in the media containing test compound at different concentrations [39]. The nanoparticles were re-suspended in the deionized water (50 mg/mL) and used as a solution with the highest concentration tested, 500 µg/mL. Morphological appearance of the

treated cells was evaluated using DM IL LED Inverted Microscope (Leica Microsystems, Wetzlar, Germany) under 20×magnification.

3. Results and discussion

Phase identification and structural analysis of the sample has been carried out by X-ray powder diffraction (XRPD). The XRPD pattern of the synthesized sample is shown in Fig. 1. As shown in the figure, the diffraction peaks assigned to α-Fe_2O_3 are strong, which indicate that the particles are well crystallized. No additional peaks have been observed in the XRPD pattern. The morphology of α-Fe_2O_3 nanoparticles has been investigated by SEM microscope. The SEM micrographs (Fig. 2(a) and (b)) of the nanoparticles show that all nanoparticles are of plate-like structure with about 10–20 nm thickness and 80–100 nm landscape length (aspect ratio ~5). Furthermore, the morphology and the structure of the samples were characterized by transmission electron microscopy (TEM). As it can be seen from lower magnification TEM images (Fig. 3(a)-(d)) the nanoparticles show well defined plate-like shapes. Careful inspection of Fig. 3(c) and Fig. 3(d) reveals that nanoparticles are composed of the core-shell structure with a thin amorphous shell of about 3-4 nm.

The crystal growth of the particle consists of two steps: nucleation and growth. These processes are affected by the interaction of intrinsic crystal structure and the external conditions. The concentration of Fe^{3+} ions during the crystal growth decreases with changes in the external conditions and influences the chemical composition and the crystal structure of the surface region. Therefore, the presence of the surface shell in the nanoplates could be due to the fact that these zones are oxygen-rich, that provoking defects and non-crystalline ordering in the α-Fe_2O_3 nanoplates.

The quantitative analysis of the core-shell structure and the shape of the hematite nanoparticles have been performed using computational methods and circularity shape descriptors [36-38]. The ratio of the core and the shell area of investigated nanoparticles were computed in the program MATLAB. To estimate accurately the area of a given shape, it was sufficient to enumerate the number of pixels inside the investigated shape. Firstly, the share (the percentage of the shell area in the core-shell nanoparticle area) of the shell in the area of nanoparticle has been determined (Fig. 4(a)-(d)). The calculated results are listed in Table 1 indicating that the share of the amorphous shell in nanoparticles is significant. Among shape descriptors, the circularity is most commonly considered for particle shape analysis in the literature [36-38,40,41]. The circularity measure is a feature of a shape that defines the degree to which a shape differs from a perfect sphere. Circularity values are assigned to sets of points which belong to the particles; these points are numbers in the range (0, 1]. The circularity measure reaches a value of 1 only in the case of a perfect circle and approaches 0 when the shape is highly non-circular, such as a line. It is desirable that circularity measure is invariant with respect to the similarity transformations of the shape, such as scaling, rotation, and translation. The measure should also be resistant to any protrusions in the shape.

Two different forms of circularity measure (roundness) can be used. Standard measure is defined as the relationship between the shape area and its perimeter

$$C_1(S) = \frac{4 \cdot \pi \cdot A}{P^2} \tag{1}$$

where A represents the shape's area and P is the shape's perimeter.

The second measure based on the calculation of particle's area is defined as following [42]. Geometric moments $m_{p,q}(S)$ for given shape S are defined as:

$$m_{p,q}(S) = \iint_S x^p \cdot y^q dxdy.$$

In the case of digitalized objects, geometric moments $m_{p,q}(S)$ are substituted by their discrete analog:

$$m_{p,q}(S) \approx \sum_{(i,j)\in S\cap Z^2} i^p \cdot j^q .$$

Since the translation of a shape changes the values of moments $m_{p,q}(S)$, it is desirable to calculate central geometric moments $\overline{m}_{p,q}(S)$ which are defined as

$$\overline{m}_{p,q}(S) = \iint_S (x - x_c(S))^p \cdot (y - y_c(S))^q dxdy$$

where the centroid $(x_c(S), y_c(S))$ of the shape *S* is given by

$$(x_c(S), y_c(S)) = \left(\frac{m_{1,0}(S)}{m_{0,0}(S)}, \frac{m_{0,1}(S)}{m_{0,0}(S)} \right).$$

The moments $\overline{m}_{p,q}(S)$ are invariant with respect to the translation, but they change under scaling, so it is preferred to use normalized moments $\mu_{p,q}(S)$ defined as

$$\mu_{p,q}(S) = \frac{\overline{m}_{p,q}(S)}{m_{0,0}(S)^{1+\frac{p+q}{2}}} .$$

Then circularity $C_2(S)$ for an arbitrary shape S whose centroid coincides with the origin is defined as:

$$C_2(S) = \frac{1}{2\pi(\mu_{2,0}(S) + \mu_{0,2}(S))}$$

Zunic *et al.* [42] showed that the so-called Hu moment $\left(\overline{m}_{2,0}(S)+\overline{m}_{0,2}(S)\right)/\left(\overline{m}_{0,0}(S)\right)^2$ reaches the minimum value of $1/(2\pi)$ only if S is a circle, and have desirable properties of C_2.

In the Table 1, values of circularity measures $C_1(S)$ and $C_2(S)$ for the core and the final core-shell structure of nanoparticle in both perspectives (perpendicular and oblique perspectives) from Fig. 4(a)-(d) are given. In the case of the nanoparticle from Fig. 4(b), both circularity measures, C_1 and C_2, indicate that the nanoparticle's core is more circular when compared with the final core-shell structure. This particle is very close to a circular shape meaning that the measure C_2 gives better results (0.9989 and 0.9966) than the measure C_1 (0.8533 and 0.8356) for circularity of core and final core-shell structure. Disadvantages of measure C_1 are caused by the fact that this measure is based on the calculation of the perimeter of nanoparticles which can significantly change when analyzing an image with noise or narrow protrusions in the shape [38]. In the case of the nanoparticle from Fig. 4(d), both circularity measures, C_1 and C_2, indicate that the nanoparticle's shell approaches the overall shape of the final core-shell structure to the ideal circle. The determined values of C_1 and C_2 in oblique perspective and perpendicular perspective presented in Table 1 clearly demonstrate the shape anisotropy of the nanoparticles.

Further, Table 1 presents the ratio of a shell area in the core-shell nanoparticle area from Fig. 4(a)-(d). The shell contains about 15% and 30% of overall core-shell nanoparticle from Fig. 4(b) and Fig. 4(d), respectively.

The field dependence of the isothermal magnetization of the as-prepared α-Fe_2O_3 nanoplates measured at room temperature is shown in Fig. 5(a). Hysteretic behavior shows a weak-ferromagnetic property of the sample at room temperature (Fig. 5(a)). The existence of the hysteresis loop, as well as the absence of the magnetization saturation, can be noticed. The

values of the coercivity, remanent magnetization, and saturation magnetization are H_C=2340 Oe, M_r=0.17 emu/g and M_S=0.53 emu/g, respectively. It is interesting that the investigated α-Fe_2O_3 plate-like nanoparticles in this work reveal higher coercivity compared with the hematite plate-like particles reported in the literature [50-53]. This observation can be assigned to the core-shell structure and plate-like morphology. The relation between particle shape and physical properties of nanosized materials has been widely studied in the literature [31,43-45]. The relationship between the shape elongation of nanoparticle and coercive field has been reported in Ref. [31,43]. For example, increasing the elongation of iron (Fe) particles by factor 5, resulted in the increase of coercivity more than 10 times (from 820 to 10100 Oe) [43]. In general, the coercive field increases with increasing elongation of the nanoparticles, i.e., with the increase of the aspect ratio. Moreover, the effect of the core-shell structure on the magnetic properties has also been reported [36,46,47]. Zhao *et al.* found that synthesized nanoplates exhibited ferromagnetic behavior at room temperature and showed that magnetization saturation was a function of the field strength [48]. The magnetization saturation (M_s), remanent magnetization (M_r) and coercivity (H_c) were about 3.12 emu g^{-1}, 0.1284 emu g^{-1}, and 34 Oe at 300 K, respectively. The observed M_r value is much higher, whereas the H_c value is much lower than those of other α-Fe_2O_3 nanoplates described in the literature. They concluded that the low H_c value may be a result of the large size of the nanoplates (≈200 nm) as well as nanoparticle increase results in the surface disorder spin decrease, leading to lower H_c values [48]. Xu *et al.* reported on coercivity of 178.9 Oe for hematite ellipsoids which is larger than that of nanospheres (141.59 Oe) or nanorhombohedra (26.1 Oe) [49]. They suggested that increase in the coercivity may have occurred due to the higher shape anisotropy for α-Fe2O3 ellipsoids [49]. Straumal *et al.* showed the importance of disordered interfaces and intergranular regions for driving high-temperature

ferromagnetism behavior [54,55]. They also concluded that the proper combination of interpenetrating crystalline and amorphous phases is the most probable condition for the existence of ferromagnetism in a pure ZnO [54,55]. Lopez-Ortega *et al.* reviewed in detail interesting core/shell nanoparticle structures with surprising magnetic properties [56]. They emphasized about the importance of core/shell structures and combination of different hard/soft and soft/hard structures, which can change magnetic parameters (M_S and H_C) in the wide range [56]. Based on these results we conclude that the surface disorder spins (amorphous shell), the size of the particles and the plate-like morphology control magnetic properties of the synthesized α-Fe_2O_3 nanoparticles.

Investigated hematite plate-like nanoparticles exhibited a low cytotoxic effect on MRC5 cells only when applied in a high concentrations of 500 μg/mL (Fig. 5(b)). The IC_{50} value was determined to be 200±9 μg/mL. Good internalization within cells was observed at 50 μg/mL (Fig. 5(c)-(d)). These nanoparticles exhibited 2.5-fold lower cytotoxicity in comparison to P400 hematite nanoparticles described recently [57]. The synthesized core-shell hematite plate-like nanoparticles presented in this study exhibited low cytotoxicity levels on the human lung fibroblasts (MRC5) cell line. These results demonstrates safe use of these nanoparticles for biomedical applications though further research is needed to ensure the full safety.

4. Conclusions

The core-shell hematite nanoplates with 10–20 nm in thickness, 80–100 nm in landscape dimensions (aspect ratio ~5) and with approximately 3-4 nm thickness of amorphous surface shell were synthesized by a hydrothermal method using ethanol, acetic acid, iron chloride, sodium hydroxide and distilled water. We used circularity measures for the quantitative shape analysis of the plate-like nanoparticles in the perpendicular (C_2~0.99) and oblique (C_2~0.55)

perspectives. The analysis confirmed strong shape anisotropy of the nanoparticles. In addition, we quantitatively estimated the share of the amorphous surface shell in an overall area of the nanoparticle. These results point to the importance of shell area in the nanoparticles. The nanoplates exhibit enhanced coercivity (H_C=2340 Oe) in comparison to other hematite plate-like structures in the literature, which can be attributed to their core-shell structure, small thicknesses (≈15 nm) and high aspect ratio of 5. Such values signify potential application of such nanoparticles in magnetic devices. Moreover, results reported herein revealed that synthesized hematite nanoplates are the material of low toxicity in the comparison to hematite samples reported in the literature [57]. We suggest that this is due to the core-shell structure where amorphous shell coats the crystal hematite nanoparticle core. We believe that the presented work, including the synthesis method, computational particle analysis, magnetic properties and cytotoxicity, will contribute to further development of the magnetic nanoparticles for practical applications.

Acknowledgement

The Ministry of Education and Science of the Republic of Serbia supported this work financially (Grants no. III 45015 and 173048). We also acknowledge financial support of bilateral project BI-RS/16-17-030.

References

[1] H. Hao, D. Sun, Y. Xu, P. Liu, G. Zhang, Y. Sun, D. Gao, J. Colloid. Interf. Sci., Hematite nanoplates: Controllable synthesis, gas sensing, photocatalytic and magnetic properties, 462 (2016) 315-324.

[2] A. Zelenakova, V. Zelenak, V. Bednarcik, P. Hrubovcak, J. Kovac, Magnetic nanocomposites of periodic mesoporous silica: The influence of the silica substrate dimensionality on the inter-particle magnetic interactions, J. Alloys Compd. 582 (2014) 483-490.

[3] A. Sivkov, E. Naiden, A. Ivashutenko, I. Shanenkov, Plasma dynamic synthesis and obtaining ultrafine powders of iron oxides with high content of ε-Fe_2O_3, J. Magn. Magn. Mater. 405 (2016) 158-168.

[4] Y. Zhao, C. Ma, C. Ma, J. Shi, J. Shi, Facile solution-free preparation of a carbon coated Fe3O4 nanoparticles/expanded graphite composite with outstanding Li-storage performances, Mater. Lett. 177 (2016) 148-151.

[5] M. Kopani, A. Kopaniova, M. Trnka, M. Caplovicova, B. Rychly, J. Jakubovsky, Cristobalite and Hematite Particles in Human Brain, Biol. Trace Elem. Res. 174 (2016) 52-57.

[6] G. Sun, H. Chen, Y. Li, G. Ma, S. Zhang, T. Jia, J. Cao, X. Wang, H. Bala, Z. Zhang, Synthesis and triethylamine sensing properties of mesoporous α-Fe_2O_3 microrods, Mater. Lett. 178 (2016) 213-216.

[7] M. Kopáni, M. Miglierini, A. Lančok, J. Dekan, M. Čaplovicová, J. Jakubovský, R. Boča, H. Mrazova, Iron oxides in human spleen, Biometals 28 (2015) 913-928.

[8] M. Tadic, S. Kralj, M. Jagodic, D. Hanzel, D. Makovec, Magnetic properties of novel superparamagnetic iron oxide nanoclusters and their peculiarity under annealing treatment, Appl. Surf. Sci. 322 (2014) 255–264.

[9] M. Tadic, M. Panjan, V. Damnjanovic, I. Milosevic, Magnetic properties of hematite (α-Fe_2O_3) nanoparticles prepared by hydrothermal synthesis method, Appl. Surf. Sci. 320 (2014) 183–187.

[10] P. Kumar, R. Kumar, H.N. Lee, Magnetic field induced one-dimensional nano/micro structures growth on the surface of iron oxide thin film, Thin Solid Films 592 (2015) 155-161.

[11] A.S. Teja, P.Y. Koh, Synthesis, properties, and applications of magnetic iron oxide nanoparticles, Prog. Cryst. Growth Charact. Mater. 55 (2009) 22-45.

[12] H.M. Yang, S. Y. Ma, G. J. Yang, W. X. Jin, T. T. Wang, X. H. Jiang, W. Q. Li, High sensitive and low concentration detection of methanol gas sensor based on one-step synthesis α-Fe_2O_3 hollow spheres, Mater. Lett. 169 (2016) 73-76.

[13] C. Wang, Z. Huang, Controlled synthesis of α-Fe_2O_3 nanostructures for efficient photocatalysis, Mater. Lett. 164 (2016) 194-197.

[14] J. Zeng, J. Li, J. Zhong, H. Yang, Y. Lu, G. Wang, Improved Sun light photocatalytic activity of α-Fe2O3 prepared with the assistance of CTAB, Mater. Lett. 160 (2015) 526-528.

[15] Q. Meng, Z. Wang, X. Chai, Z. Weng, R. Ding, L. Dong, Fabrication of hematite (α-Fe2O3) nanoparticles using electrochemical deposition, Appl. Surf. Sci. 368 (2016) 303-308.

[16] J. Tomaszewska, S. Jakubiak, J. Michalski, W. Pronk, S.J. Hug, K.J. Kurzydłowski, A polypropylene cartridge filter with hematite nanoparticles for solid particles retention and arsenic removal, Appl. Surf. Sci. 366 (2016) 529-534.

[17] C. Zheng, Z. Zhu, S. Wang, Y. Hou, NaF-assisted hydrothermal synthesis of Ti-doped hematite nanocubes with enhanced photoelectrochemical activity for water splitting, Appl. Surf. Sci. 359 (2015) 805-811.

[18] A. Pu, J. Deng, Y. Hao, X. Sun, J. Zhong, Thickness effect of hematite nanostructures prepared by hydrothermal method for solar water splitting, Appl. Surf. Sci. 320 (2014) 213-217.

[19] N. Saveh-Shemshaki, M. Latifi, R. Bagherzadeh, M. Malekshahi Byranvand, N. Naseri, A. Dabirian, Synthesis of mesoporous functional hematite nanofibrous photoanodes by electrospinning, Polym. Advan. Technol. 27 (2016) 358-365.

[20] H. Wan, T. Liu, X. Liu, J. Pan, N. Zhang, R. Ma, H. Wang, G. Qiu, Acetates-induced controlled-synthesis of hematite polyhedra enclosed by high-activity facets for enhanced photocatalytic performance, RSC Adv. 6 (2016) 66879-66883.

[21] R. Kant, N. Kumar, V. Dutta, Fabrication of micro/nanostructured α-Fe_2O_3 hollow spheres: effect of electric field on the morphological, magnetic and photocatalytic properties, RSC Adv. 6 (2016) 65789-65798.

[22] K.W. Kim, S.W. Lee, Facile synthesis of chitosan-mediated hematite clusters as an efficient photocatalyst, Sci. Adv. Mater. 8 (2016) 180-184.

[23] N.M. Hosny, N. Nowesser, A.S. Al Hussaini, M.S. Zoromba, Solid state synthesis of hematite nanoparticles from doped poly o-aminophenol (POAP), J. Inorg. Organomet. P. 26 (2016) 41-47.

[24] M.K. Bayazit, E. Cao, A. Gavriilidis, J. Tang, A microwave promoted continuous flow approach to self-assembled hierarchical hematite superstructures, Green Chem. 18 (2016) 3057-3065.

[25] A. Bhattacharjee, A., Rooj, M. Roy, J. Kusz, P. Gutlich, Solventless synthesis of hematite nanoparticles using ferrocene, J. Mater. Sci. 48 (2013) 2961-2968.

[26] M. Nidhin, K.J. Sreeram, B.U. Nair, Polysaccharide films as templates in the synthesis of hematite nanostructures with special properties Appl. Surf. Sci. 258 (2012) 5179-5184.

[27] S.B. Wang, Y.L. Min, S.H. Yu, Synthesis and magnetic properties of uniform hematite nanocubes, J. Phys. Chem.y C 111 (2007) 3551-3554.

[28] L. Diamandescu, D. Mihaila-Tarabasanu, N. Popescu-Pogrion, A. Totovina, I. Bibicu, Hydrothermal synthesis and characterization of some polycrystalline α-iron oxides, Ceram. Int. 25 (1999) 689-692.

[29] M. Tadic, D. Markovic , V. Spasojevic, V. Kusigerski, M. Remskar, J. Pirnat, Z. Jaglicic, Synthesis and magnetic properties of concentrated α-Fe_2O_3 nanoparticles in a silica matrix, J. Alloys Compd. 441 (2007) 291–296.

[30] M. Tadic, V. Kusigerski, D. Markovic, I. Milosevic, V. Spasojevic, High concentration of hematite nanoparticles in a silica matrix: Structural and magnetic properties, J. Mag. Mag. Mater. 321 (2009) 12–16.

[31] J. Jayashainy, P. Sagayaraj, Investigation on the shape evolution of 1D mesoporous hematite nanoparticles prepared via anion-assisted hydrothermal approach, J. Alloys Compd. 626 (2015) 323-329.

[32] M. Roy, M.K. Naskar, Alkali metal ions induced cube shaped mesoporous hematite particles for improved magnetic properties, and efficient degradation of water pollutant, Phys. Chem. Chem. Phys. DOI: 10.1039/c6cp02442d.

[33] Z. Li, X. Lai, H. Wang, D. Mao, C. Xing, D. Wang, Direct hydrothermal synthesis of single-crystalline hematite nanorods assisted by 1, 2-propanediamine, Nanotechnology 20 (2009) 245603–245611.

[34] C.R. Murthy, B. Gao, A.R. Tao, G. Arya, Automated quantitative image analysis of nanoparticle assembly, Nanoscale 7 (2015) 9793-9805.

[35] C.R. Laramy, K.A. Brown, M.N. O'Brien, C.A. Mirkin, High-Throughput, Algorithmic Determination of Nanoparticle Structure from Electron Microscopy Images, ACS Nano 9 (2015) 12488-12495.

[36] L. Kopanja, S. Kralj, D. Zunic, B. Loncar, M. Tadic, Core–shell superparamagnetic iron oxide nanoparticle (SPION) clusters: TEM micrograph analysis, particle design and shape analysis, Ceram. Int. 42 (2016) 10976-10984.

[37] L. Kopanja, I. Milosevic, M. Panjan, V. Damnjanovic, M. Tadic, Sol–gel combustion synthesis, particle shape analysis and magnetic properties of hematite (α-Fe_2O_3) nanoparticles embedded in an amorphous silica matrix, Appl. Surf. Sci. 362 (2016) 380-386.

[38] L. Kopanja, D. Žunić, B. Lončar, S. Gyergyek, M. Tadić, Quantifying shapes of nanoparticles using modified circularity and ellipticity measures, Measurement 92 (2016) 252-263.

[39] M.B. Hansen, S.E. Nielsen, K. Berg, Re-examination and further development of a precise and rapid dye method for measuring cell growth/cell kill, J. Immunol. Meth 119 (1989) 203-210.

[40] G. Muscas, G. Singh, W.R. Glomm, R. Mathieu, P.A. Kumar, G. Concas, et al., Tuning the size and shape of oxide nanoparticles by controlling oxygen content in the reaction environment: morphological analysis by aspect maps, Chem. Mater. 27 (2015) 1982–1990.

[41] J. Žunić, K. Hirota, P. L. Rosin, Note on the shape circularity measure method based on radial moments, Journal of Electronic Imaging, 23 (2014) 029701.

[42] J. Žunić, K. Hirota, P. L. Rosin, A Hu moment invariant as a shape circularity measure, Pattern Recognit. 43 (2010) 47–57.

[43] A.-H. Lu, E.L. Salabas, F. Schüth, Magnetic nanoparticles: synthesis, protection, functionalization, and application, Angew. Chem. Int. Ed. Engl. 46 (2007) 1222–1244.

[44] T.O. Paine, L.I. Mendelsohn, F.E. Luborsky, Effect of shape anisotropy on the coercive force of elongated single-magnetic-domain iron particles, Phys. Rev. 100 (1955) 1055–1059.

[45] L. Liu, H.-Z. Kou, W. Mo, H. Liu, Y. Wang, Surfactant-assisted synthesis of alphaFe2O3 nanotubes and nanorods with shape-dependent magnetic properties, J. Phys. Chem. B 110 (2006) 15218–15223.

[46] M. Ito, M. Yano, N. Sakuma, H. Kishimoto, A. Manabe, T. Shoji, A. Kato, N. M. Dempsey, D. Givord, and G. T. Zimanyi, Coercivity enhancement in Ce-Fe-B based magnets by core-shell grain structuring, AIP Adv. 6 (2016) 056029.

[47] V. Zelenak, A. Zelenakova, J. Kovac, U. Vainio, N. Murafa, Influence of Surface Effects on Magnetic Behavior of Hematite Nanoparticles Embedded in Porous Silica Matrix, J. Phys. Chem. C 113 (2009) 13045–13050.

[48] J. Zhao, P. Yang, H.S. Chen, J. Li, Q. Che, Y. Zhu, R. Shi, Effect of sequential morphology adjustment of hematite nanoplates to nanospindles on their properties and applications, J. Mater. Chem. C 3 (2015) 2539-2547.

[49] C. Xu, Y. Wang, H. Chen, Facile synthesis of ellipsoidal hematite nanostructures via an EDA-assisted solvothermal method, J. Mater Sci-Mater. El. 26 (2015) 5446-5450.

[50] J. Cai, S. Chen, M. Ji, J. Hu, Y. Ma, L. Qi, Organic additive-free synthesis of mesocrystalline hematite nanoplates via two-dimensional oriented attachment, CrystEngComm 16 (2014) 1553-1559.

[51] J. Zhao, P. Yang, H.-S. Chen, J. Li, Q. Che, Y. Zhu, R. Shi, Effect of sequential morphology adjustment of hematite nanoplates to nanospindles on their properties and applications, J. Mater. Chem. C 3 (2015) 2539-2547.

[52] H. Hao, D. Sun, Y. Xu, P. Liu, G. Zhang, Y. Sun, D. Gao, Hematite nanoplates: Controllable synthesis, gas sensing, photocatalytic and magnetic properties, J. Colloid. Interf. Sci. 462 (2016) 315-324.

[53] M. Tadić, N. Čitaković, M. Panjan, Z. Stojanović, D. Marković, V. Spasojević, Synthesis, morphology, microstructure and magnetic properties of hematite submicron particles, J. Alloys Compd. 509 (2011) 7639-7644.

[54] B.B. Straumal, S.G. Protasova, A.A. Mazilkin, B. Baretzky, A.A. Myatiev, P.B. Straumal, T. Tietze, G. Schütz, E. Goering, Amorphous interlayers between crystalline grains in ferromagnetic ZnO films, Mater. Lett. 71 (2012) 21-24.

[55] T. Tietze, P. Audehm, Y.C. Chen, G. Schütz, B.B. Straumal, S.G. Protasova, A.A. Mazilkin, P.B. Straumal, T. Prokscha, H. Luetkens, Z. Salman, Interfacial dominated ferromagnetism in nanograined ZnO: a μSR and DFT study, Sci. Rep. 5 (2015) 8871.

[56] A. Lopez-Ortega, M. Estrader, G. Salazar-Alvarez, A.G. Roca, J. Nogues, Applications of exchange coupled bi-magnetic hard/soft and soft/hard magnetic core/shell nanoparticles, Physics Reports 553 (2015) 1-32.

[57] D. Cardillo, M. Tehei, Md.S. Hossain, Md.M. Islam, K. Bogusz, D. Shi, D. Mitchell, M. Lerch, A. Rosenfeld, S. Corde, K. Konstantinov, Synthesis-dependent surface defects and morphology of hematite nanoparticles and their effect on cytotoxicity in vitro, ACS Appl. Mater. Inter. 8 (2016) 5867-5876.

Figure caption:

Figure 1. X-ray diffraction pattern of the sample. The Miller indices (hkl) of the peaks are also shown.

Figure 2. SEM images of the plate-like α-Fe_2O_3 nanoparticles.

Figure 3. (a)–(d) Transmission electron micrographs of the plate-like α-Fe_2O_3 nanoparticles: selected regions of the perpendicular perspective and selected regions of the oblique perspective.

Figure 4. TEM images of the single plate-like nanoparticles and their isolated core-shell nanoparticles after segmentation procedure.

Figure 5. (a) The hysteresis loop of the hematite nanoparticles at room temperature; Cytotoxicity profile of the nanoparticles on MRC5 cell line: (b) dose response and (c)-(d) morphological cell appearance after 48 h treatment.

Figure 1

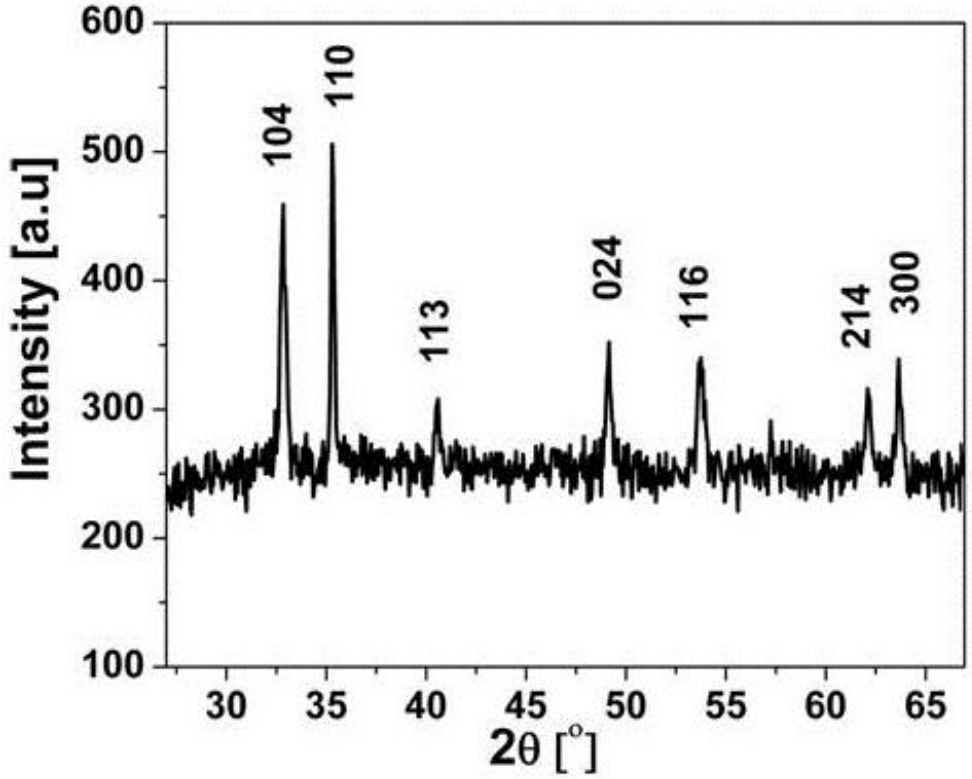

Figure 2

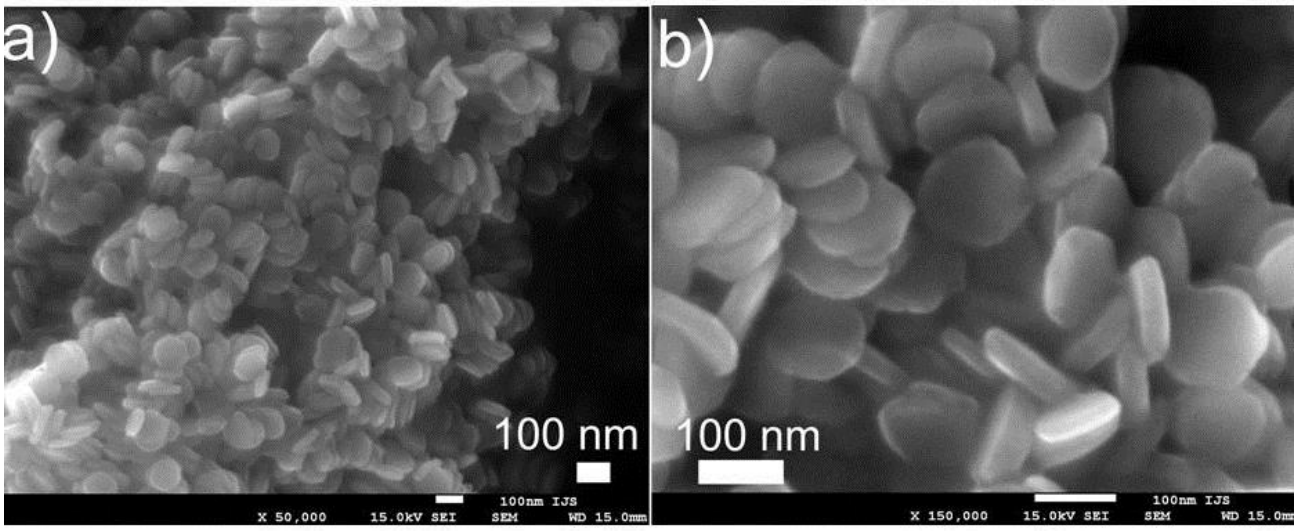

Figure 3

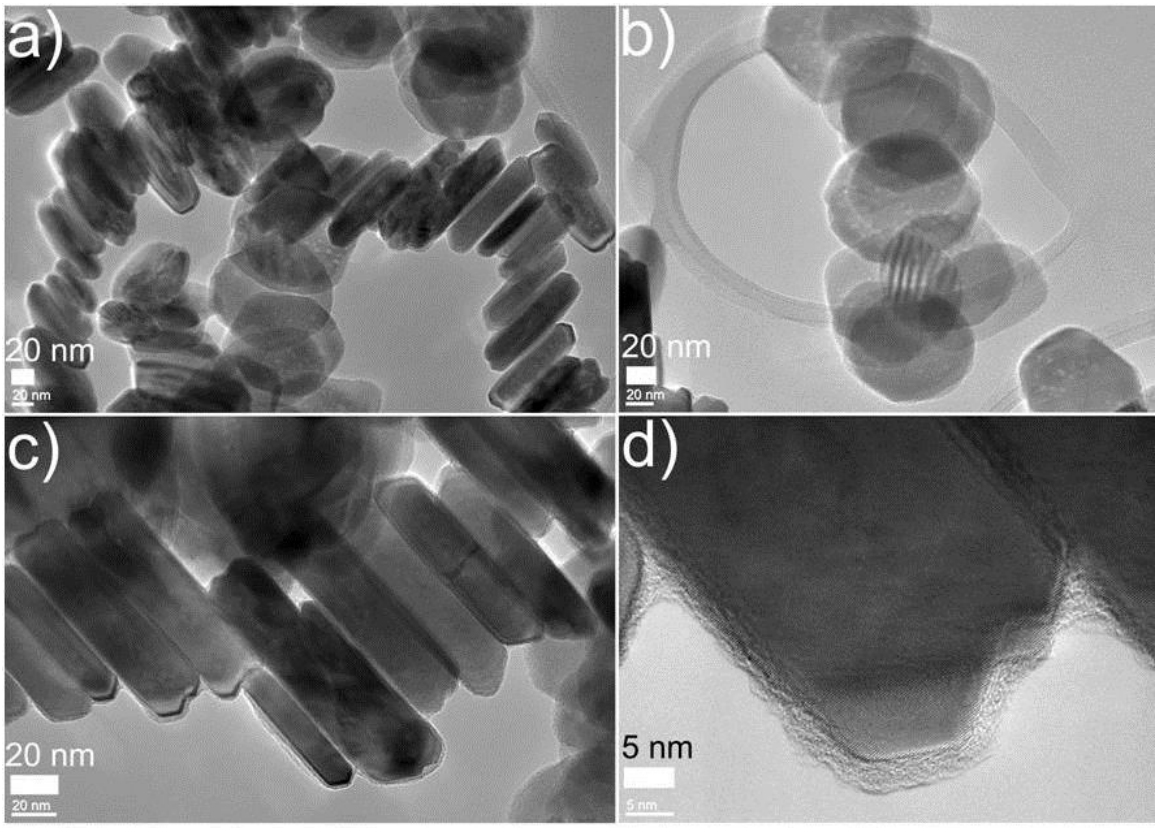

Figure 4

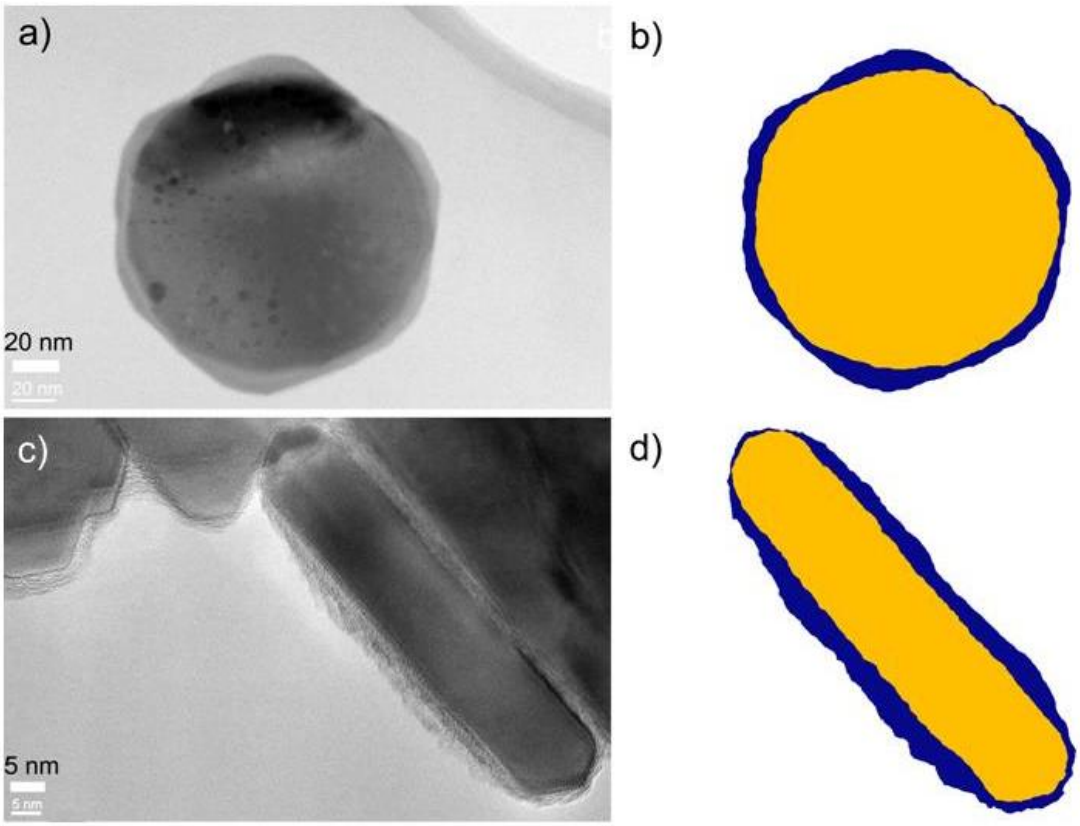

Figure 5

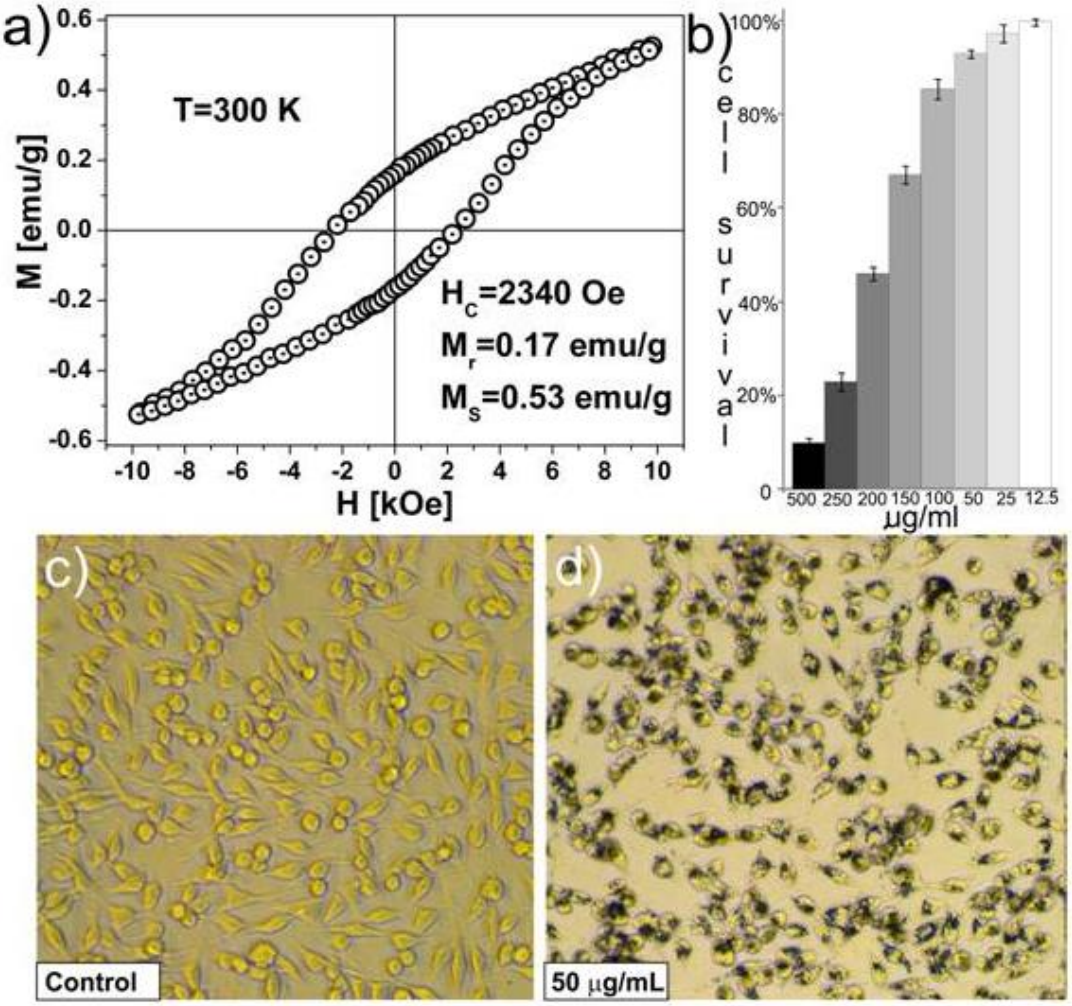

Table 1. Overview analysis results of the plate-like hematite nanoparticles.

	the perpendicular perspective (Fig.4(a) and (b))	the oblique perspective (Fig.4(c) and (d))
The percentage of the shell area in the core-shell nanoparticle area [%]	14.99%	29.70%
C_1 *(core)*	0.8533	0.4115
C_1 *(core-shell)*	0.8356	0.5073
C_2 *(core)*	0.9989	0.3938
C_2 *(core-shell)*	0.9966	0.5458